Journal of Ethnopharmacology 283 (2022) 114706

Contents lists available at ScienceDirect

Journal of Ethnopharmacology

journal homepage: www.elsevier.com/locate/jethpharm

The anti-tumor effect of OP-B on ovarian cancer in vitro and in vivo, and its mechanism: An investigation using network pharmacology-based analysis

Shuang Yuan [a,b], Yuanyuan Xu [a,b], Tao Yi [b,*], Hongjing Wang [a,b,**]

[a] Department of Gynecology and Obstetrics, West China Second University Hospital, Sichuan University, Chengdu, Sichuan, 610041, China
[b] Key Laboratory of Birth Defects and Related Diseases of Women and Children (Sichuan University), Ministry of Education, Chengdu, Sichuan, 610041, China

ARTICLE INFO

Keywords:
Ophiopogonin B
Ovarian cancer
Network pharmacology
STAT3 pathway

ABSTRACT

Ethnopharmacological relevance: Maidong (Liliaceae) is used as a yin-nourishing medication for the treatment of cardiovascular disease, inflammation, and assistant cancer chemotherapy in the clinic. Ophiopogonin B (OP-B), a major saponin extracted from Maidong, is reported to have potential antitumor activities against various human cancers. However, the effects of OP-B on human ovarian cancer (OC) and the potential mechanisms of action are yet elusive.

Aim of the study: In this study, we aimed to explore the potential molecular mechanisms of OP-B in the treatment of OC using network pharmacology. In vivo and in vitro experiments were conducted to further verify the therapeutic effects of OP-B on OC.

Materials and methods: To investigate the functions of OP-B against OC holistically, the related targets of OP-B and OC were each predicted based on four public databases. Subsequently, the identified PPI network was constructed to detect the hub potential targets. In addition, GO and KEGG enrichment analysis were applied by Metascape database. Furthermore, we simultaneously investigated the anticancer effects of OP-B on SKOV3 and A2780 human ovarian cancer cells using a cell viability assay, transwell assay, and an image-based cytometric assay. The quantitative real-time PCR and western-blot assay were used to validate the RNA and protein levels of target genes in OP-B treated OC cells. At last, SKOV3-bearing BALB/c nude mice were applied to observe the effectiveness and toxicity of OP-B.

Results: Through network pharmacological analysis, OP-B was found to play a critical role in OC via multiple targets and pathways, especially the STAT3 signaling pathways. In addition, in vitro experiments found OP-B suppressed SKOV3 and A2780 cells proliferation in a time and concentration dependent manner, and markedly impaired cancer cell migration. Flow cytometry analysis revealed that OP-B significantly increased early and late apoptosis, induced G2/M phase cell cycle arrest in SKOV3 cells and G0/G1 phase cell cycle arrest in A2780 cells. Moreover, OP-B administration down-regulated the expression of p-STAT3 protein, whereas the RNA expression and total protein levels of STAT3 were not altered. Finally, in vivo experiments confirmed the therapeutic effects of OP-B on OC in nude mice with low toxicity in heart, liver, lung, and kidney.

Conclusion: OP-B could efficiently suppress OC cellular proliferation, migration and induce apoptosis, cell cycle arrest mainly via the regulation of STAT3 signaling pathway. This study provides a promising potential application for an alternative to chemotherapy in ovarian cancer.

1. Introduction

Ovarian cancer (OC) is a highly metastatic and lethal disease among gynecological malignancies with 294,414 new cases and 184,799 deaths worldwide in 2020 (Siegel et al., 2020). The most common subtype among ovarian cancer malignancies is high-grade serous ovarian cancer which accounts for ~70% of all OC presentations. The current standard treatment for OC includes staging/cytoreductive surgery combined with platinum-based adjuvant chemotherapy. The first-line chemotherapy drugs are carboplatin and paclitaxel (Lheureux et al., 2019). OC is characterized by insidious symptoms, high metastasis, lack of efficient screening methods and biomarkers, thus, 3 out of 4 patients are in advanced stage (FIGO III/IV) at diagnosis (Armstrong et al., 2021). Due

* Corresponding author.
** Corresponding author. Department of Gynecology and Obstetrics, West China Second University Hospital, Sichuan University, China.
E-mail addresses: yitao@scu.edu.cn (T. Yi), whjscdx@163.com (H. Wang).

https://doi.org/10.1016/j.jep.2021.114706
Received 4 July 2021; Received in revised form 17 September 2021; Accepted 1 October 2021
Available online 3 October 2021

List of abbreviation

OP-B	Ophiopogonin B
OC	ovarian cancer
FIGO	international federation of Gynecology and Obstetrics
DMSO	dimethyl sulfoxide
FBS	fetal bovine serum
PBS	phosphate buffered saline
Annexin V-FITC	Annexin V-fluorescein isothiocyanate
PI	propidium iodide
PMSF	phenylmethanesulfonylfluoride
qRT-PCR	quantitative real-time polymerase chain reaction
PVDF	polyvinylidene fluoride
HRP	horseradish peroxidase
GO	gene ontology
KEGG	Kyoto encyclopedia of genes and genomes
PPI	protein-protein interaction
BP	biological process
MF	molecular function
CC	cell composition
EPC	edge percolated component
MNC	maximum neighborhood component
MCC	maximal clique centrality
JAK2	Janus kinase 2
STAT3	signal transducers and activators of transcription

to tumor recurrence and acquired chemoresistance, the 5-year and 10-year overall survival rates of advanced OC are only 32% and 15% (Sung et al., 2021). Moreover, common chemotherapy drugs have a high incidence of side-effects, which seriously affects the quality of life of patients (Kuroki and Guntupalli, 2020). Progress in the treatment of OC has seen with the introduction of targeted therapies, such as bevacizumab and ploy (ADP-ribose) polymerase inhibitors, and a plethora of immunotherapy trials (Lee et al., 2019). However, targeted drugs are expensive and the choice is often limited. Numerous acquired drug-resistant cases arise after long-term drug administration. Therefore, exploration of new effective, safe, and cheap therapeutic drugs in OC is urgently needed.

Natural compounds, especially plant-derived compounds, have been widely used as alternative or adjuvant therapeutic agents against cancer, with the advantages of multi-target, inexpensive, accessible and low toxicity (Demain and Vaishnav, 2011). The list of examples includes Taxol, vincristine, penicillin and vinblastine as leading drugs in the market from natural sources (Deorukhkar et al., 2007). Maidong, also known as Ophiopogon japonicus (L.f.) Ker-Gawl, is an evergreen perennial in the Liliaceae family and a famous Chinese traditional medicinal herb. Maidong is used to nourish Yin, moisten the lungs, clean the heart-fire, and promote fluid production (M.-H. Chen et al., 2016b). It is one of the main components of commercially available Chinese patent medicines, such as Shenmai injection, which is widely used medication in viral myocarditis, coronary heart disease, neutropenia and cancer chemotherapy (Lu et al., 2014). Modern phytochemical research has revealed that Maidong contains various components, of which steroidal saponins are the eminent members (Zhao et al., 2017). More than 70 different types of spirosteroid and furostanol saponins have been identified, including Ophiopogonin B, D, D′ (Lyu et al., 2020). Ophiopogonin saponins have been demonstrated to have a wide range of pharmacological properties, such as cardiovascular protection, anti-tumor, anti-inflammatory and anti-radiation activities. Among them all, Ophiopogonin B(OP-B) is considered to be one of the most active and abundant steroid saponins, with broad-spectrum anti-tumor effects.

Previous studies show that OP-B inhibits the growth of non-small cell lung cancer (Chen et al., 2018), gastric cancer (Zhang et al., 2016), colon cancer (Gao et al., 2018), and cervical cancer (Xu et al., 2013). OP-B is a typical multi-target drug. Current pharmacological studies have found that the anti-tumor mechanism of OP-B is closely related to the following pathways (Yan et al., 2020): (1) Reducing the ratio of Bcl-2/Bax and activating the Caspase protein Family to promote cell apoptosis; (2) Interacting with cyclins and cyclin-dependent kinases, and then participate in cell cycle arrest and disrupt cell mitosis; (3) Inhibiting related proteins such as MMPs, MAPK, TNF-α, STAT3 expression to reduce tumor cell adhesion, invasion, and metastasis capacity; (4) Inhibiting PI3K/Akt/mTOR pathway to induce tumor cell autophagy (He et al., 2018). Therefore, OP-B has become the prospect for the development of new antitumor drugs. However, the impacts of OP-B on OC and related molecular mechanisms are yet elusive.

As the advancement in bioinformatics field, network pharmacology has improved significantly for drug discovery and their design processes (Kibble et al., 2015). Network pharmacology is a cross-discipline which is based on systems biology and combines poly-pharmacology, molecular network data, bioinformatics, and computer simulation (Chen et al., 2016c). Moreover, the predictive results of the network pharmacology could provide the rationale for further research directions in new drug investigation. Thus, network pharmacology is well suited for analyzing the multi-targeted agents, which helps to advance the process of drug discovery with less time and economic cost. So It may be appropriate for identifying the complex mechanisms of OP-B.

In this study, network pharmacology was conducted to establish the targets-disease network to investigate the core targets and biological functions, pathways, and mechanisms of OP-B in treating OC. And then, Cell experiments and xenograft models were conducted to explore the anti-tumor effect of OP-B on OC (Fig. 1).

2. Materials and methods

2.1. Network pharmacological analysis

2.1.1. Predicted targets of OP-B

The related targets of OP-B were aggregated from SwissTargetPrediction (http://www.swisstargetprediction.ch/) and PharmMapper (http://www.lilab-ecust.cn/pharmmapper/) databases. Chemical structure saved as "sdf" files was gathered from PubChem (https://pubchem.ncbi.nlm.nih.gov/). The presumed gene symbol names were manual normalised in the UniprotKB database (https://www.UniProt.org/).

2.1.2. Potential target genes of OC

The OC associated target genes were obtained from DisGeNET (https://www.disgenet.org/)and Genecards database (https://www.genecards.org/) . Search strategy: Set the keyword as "Ovarian Carcinoma" or "ovarian cancer". The species was set to *Homo sapiens*.

2.1.3. Network construction

In order to clarify the interaction between the drug-related targets of OP-B and the targets of OC, the Venn online software Bioinformatics & Evolutionary Genomics (http://bioinformatics.psb.ugent.be/webtools/Venn/) was used to take intersection and draw the Venn diagram. Then submit the intersection target to the STRING 11.0 database (https://string-db.org) to construct a protein-protein interaction (PPI) network model, set the biological species to "*Homo sapiens*", and the minimum interaction threshold to "high confidence" (>0.7). Further analyze the Hub gene in the network through the CytoHubba plug-in in CytoScape (3.7.2).

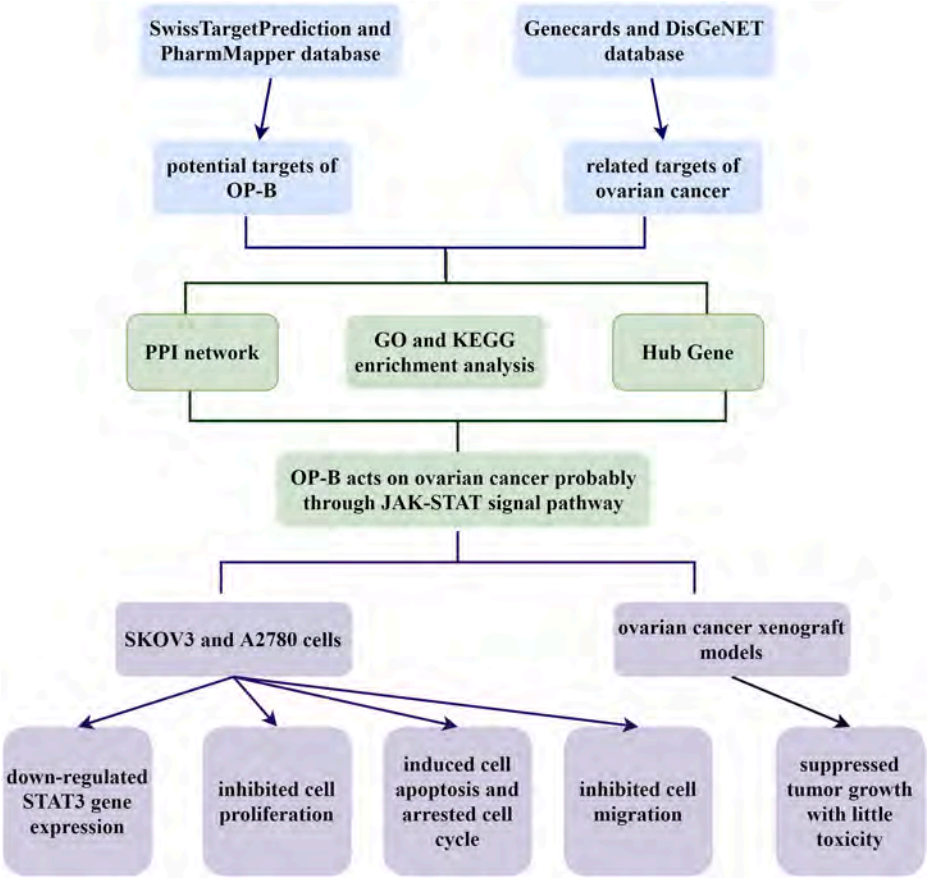

Fig. 1. Flowchart.

2.1.4. Enrichment analysis

Gene Ontology (GO) analysis and Kyoto Encyclopedia of Genes and Genomes (KEGG) Pathway Enrichment Analysis were used to explore the biological pathways and potential functions. Enter the intersection target into the Metascape platform (http://metascape.org/gp/index.html#/main/step1), set $P < 0.01$, analyze the main biological processes and metabolic pathways and perform enrichment analysis, save the results, and use the Hiplot (https://hiplot.com.cn/) online tools to visualize the data.

2.2. Pharmacological verification on network analysis

2.2.1. Reagents

Ophiopogonin B (OP-B) (MW: 722.9, HPLC ≥98%) was purchased from Shanghai Yuanye Bio-Technology Co., Ltd (Shanghai, China). Cisplatin (MW: 300.05, HPLC ≥99%) was purchased from MedChemExpress (Shanghai, China). Stock solutions of the compounds were freshly prepared in dimethylsulfoxide (DMSO). Antibodies, including anti-STAT3, anti-β-actin, HRP conjugated goat anti-rabbit IgG were from Abways Technology (Chengdu, China). Anti-p-STAT3 was obtained from Cell Signaling Technology (Boston, USA).

2.2.2. Cell culture

The human ovarian cancer cell lines (SKOV3 and A2780) were obtained from Key Laboratory of Birth Defects and Related Diseases of Women and Children (Sichuan University), Ministry of Education. The SKOV3 and A2780 cells were cultured in Dulbecco's modified Eagle's medium (DMEM), supplemented with 10% fetal bovine serum (FBS; Gibco, Waltham, Ma, USA), 100 U/ml penicillin-streptomycin mixed antibiotics at 37 °C in a humidified 5% CO2 incubator.

2.2.3. Cell viability assay

The cell viability of SKOV3 and A2780 cells was evaluated using the CellTiter 96® AQ_{ueous} One Solution Cell Proliferation Assay (promega, Medison, WI, USA). Briefly, cells with a density of 8×10^3 or 4×10^3 cells/100 μL were seeded onto 96-well plates. After cell attachment, 10, 20, 30, 40 μM OP-B and Cisplatin were added. 1‰ DMSO was used as a negative control and Cisplatin as the positive control. After treatment for 24, 48h, 20 μL of CellTiter 96® AQ_{ueous} One Solution Reagent was added and incubated for 1 h. The absorbance was measured at 490 nm (CMax Plus; Molecular Devices, Shanghai, China). All experiments were done using five replicates and repeated at least three times. Viability of negative control was taken as 100%.

2.2.4. Transwell assay

Cell migration assay was performed in a 24-well Transwell (Corning, NY, USA) on a polycarbonate filter (8.0 mm pore size). In brief, SKOV3 and A2780 cells were, respectively, cultured in the presence of 15, 20 μM OP-B or 1‰ DMSO (negative control) for 24 h, and then 4×10^4/200 μL SKOV3 and 1×10^5/200 μL A2780 cells were seeded into the upper chambers. The lower chamber was filled with 600 μL of medium supplemented with 10% FBS. After incubation at 37 °C for 24 h, cells on the upper chamber were removed by a cotton swab. Migrated cells on the bottom of the membranes were fixed with 4% paraformaldehyde and stained with 0.1% crystal violet solution, and then photographed under the microscope. Cell numbers were counted by ImageJ 1.8.0 software in five randomly selected fields at 200-fold magnification.

2.2.5. Cell apoptosis assay

The cell apoptosis rate of SKOV3 and A2780 cells was evaluated using Annexin V-Fluorescein Isothiocyanate/Propidium Iodide (Annexin V-FITC/PI) apoptosis kit (Yeasen Biotechnology Co., Ltd.,

Shanghai, China). Briefly, cells with a density of 2×10^5 or 1.5×10^5 cells/2 mL were seeded onto 6-well plates. After cell attachment, 10, 20, 30 μM OP-B were added. 1‰ DMSO was used as a negative control. After incubation for 24, 48h, cells were harvested by centrifugation and sequentially mixed with 100 μl Binding buffer, Annexin V-FITC (5 μL) and PI (10 μL). The reaction mixture was placed in a dark place for 5–15 min at 4 °C, then transferred to the 96-well plates for analysis (Millipore guava, Merck, Germany).

2.2.6. Cell cycle assay

The cell cycle distribution of SKOV3 and A2780 cells was evaluated using PI Cell Cycle Detection kit (KeyGEN, Jiangsu, China). Briefly, cells with a density of 2×10^5 or 1.5×10^5 cells/2 mL were seeded onto 6-well plates. After serum starvation, cells were treated with 10, 20, 30 μM OP-B for 24 h. 1‰ DMSO was used as a negative control. The cells were collected and fixed in ice-cold 70% ethanol at 4 °C overnight. Then washed the cells and added 50 μL RNase and 450 μL PI mixture for 30 min at 25 °C. The distribution of cell cycle (subG1, G0/G1, S and G2/M) was measured by flow cytometry (FC500, Beckman Coulter, USA).

2.2.7. Quantitative real-time PCR (qRT-PCR)

Total RNA was extracted after 24 h incubation with 20 μM OP-B or 1‰ DMSO (negative control) using TRIzol reagent (CWBIO, Beijing, China) according to the manufacturer's instructions. After purification and quantification, RNA was determined by measuring optical density at 260 and 280 nm by nanodrop (NanoDrop-ND-1000). Reverse transcription was performed using 1 μg RNA, and HiScript III RT SuperMix (Vazyme Biotech, Nanjing, China). cDNA was diluted 8 times for qPCR analysis. qPCR was performed with a CFX96 Touch Real-Time PCR Detection System (Bio-rad, Hercules, CA, USA) using Hieff UNICON® Universal Blue qPCR SYBR Green Master Mix. The primers for qPCR were designed and synthesized by Sangon Biotech (Shanghai) Co., Ltd. as follows: β-actin: 5′- GCACCACACCTTCTACAATGAG -3' (forward) and 5′- ACAGCCTGGATGGCTACGT -3' (reverse); STAT3: 5′-AGCAAAGAATCACATGCCACT-3' (forward) and 5′- CCATTGGCTTCTCAAGATACCTG -3' (reverse). All qPCR experiments were performed in triplicate, and the mean value was used for to determine the messenger RNA (mRNA) levels. Relative quantification of the mRNA levels was performed using the comparative Ct method with β-actin as the reference gene and using the $2^{-\Delta\Delta Ct}$ formula.

2.2.8. Western blot analysis

Cell proteins were extracted after 24 h incubation with 20 μM OP-B or 1‰ DMSO (negative control) using RIPA lysis buffer (CWBIO, Beijing, China) containing 100 × PMSF. Protein concentrations were determined by the BCA assay (Beyotime, Shanghai, China). Sample proteins were loaded and electrophoresis separated by 4%–20% Precast Protein Improve Gels. After wet transfer using 0.45 μm PVDF membranes. The membranes were blocked and incubated with appropriate primary antibodies against STAT3, p-STAT3 and β-actin overnight at 4 °C, and then with HRP-conjugated anti-rabbit IgG for an additional hour at room temperature. At last, enhanced chemiluminescence was performed to visualize the bands (ECL; Beyotime, Shanghai, China). Image acquisition was performed using Image Lab software.

2.2.9. Nude mouse xenografts

Ethical clearance was approved by the Research Ethics Committee of West China Second University Hospital, Sichuan University. Five-week-old athymic BALB/c mice were purchased from Vital River Laboratory Animal Technology Company (Beijing, China). All mice were maintained at 25 ± 2 °C and relative humidity (40–60%) on a 12 h light/dark cycle with free access to food and water. After one week of habituation, exponentially growing SKOV3 cells ($1x10^7$ in 0.2 ml PBS) were subcutaneously injected into the right dorsal scapula area of the mice. After successful modeling, tumor-bearing mice were divided into three groups randomly, which were treated by intragastric administration with OP-B (15 or 75 mg/kg daily; n=5) or saline (negative control, daily; n=5). Tumor growth was determined by measuring the tumor volume (length × width^2 × 0.5) every 3 days. The mice were euthanized at the end of the experiment (medication for 21 days), and the tumors were excised, photographed and weighed. The tumor inhibition ratio was calculated as follows: (1 – OP-B group tumor weight/control group tumor weight) × 100%. The pathological status of heart, liver, lung, and renal tissues were confirmed with H&E staining and pathological examination.

2.3. Statistical analysis

All data were first subjected to normality test and expressed as mean ± standard deviation. According to the results of homogeneity of variance, the data of cell viability, tumor volume, body weight of nude mice were analyzed by repeated measures analysis of variance (ANOVA); the data of qPCR and Western blot were analyzed by T tests; and other data were statistically analyzed using one-way ANOVA (SPSS 25.0). Dunnett's test was followed when compare the experiment groups and control group. Statistical graphs were generated using GraphPad Prism 8.02. $p < 0.05$ was defined as significant.

3. Results

3.1. Targets genes of OP-B and OC

In this study, 13 targets were acquired from the SwissTargetPrediction database (confidence probability >0). 290 targets were acquired from the PharmMapper database (Norm Fit score >0). After merging the hit lists and removing duplicates, 296 unique hits remained as potential targets of OP-B. The number of targets collected from DisGeNET and Genecards databases, were 30 and 447, respectively. In total, 449 genes were identified as OC-related genes following gene name standardization and de-duplication.

3.2. PPI network analysis

A total of 55 common targets were obtained with the Venn diagram (Fig. 2A). The PPI network was constructed via STRING v11.0 with threshold 'high confidence (> 0.7)' and visualized with Cytoscape software (Fig. 2B). This PPI network included 54 nodes and 337 edges, with an average node degree of 12.5, a network diameter of 5, and an average number of 12.481 neighbors. The circular node represents each protein, The bigger the node size is, the higher the degree value is. And the straight line between the nodes represents the interaction between the two proteins. The thicker the line is, the stronger the interaction is. Hub genes are calculated by cytoHubba plugin. Use MCC, MNC, EPC, Degree, closeness, and Radiality methods to calculate top ten hub genes, and take the intersection of the results to get 10 hub genes. Those are STAT3, MAPK1, AKT1, MAPK8, SRC, EGFR, IGF1, PIK3R1, HRAS, JAK2.

3.3. Enrichment analysis

In order to explore the biological functions of the intersection genes, we performed two kinds of enrichment analyses using Metascape: (a) GO enrichment analyze and (b) KEGG enrichment analyze. The biological processes that OP-B mainly participates in include transmembrane receptor protein tyrosine kinase signaling pathway, apoptotic signaling pathway, cellular response to organic cyclic compound, regulation of cell adhesion, positive regulation of cell death etc., (Fig. 2C). The molecular functions are mainly enriched in kinase binding, protein kinase activity, transcription factor binding, protein homodimerization activity, nuclear receptor activity etc., (Fig. 2C). The main pathways involved are Pathways in cancer, Proteoglycans in cancer, Platinum drug resistance, Jak-STAT signaling pathway, Endocytosis, Transcriptional misregulation in cancer, Oocyte meiosis, Apoptosis - multiple species, Cell cycle, Mitophagy – animal etc., (Fig. 2D).

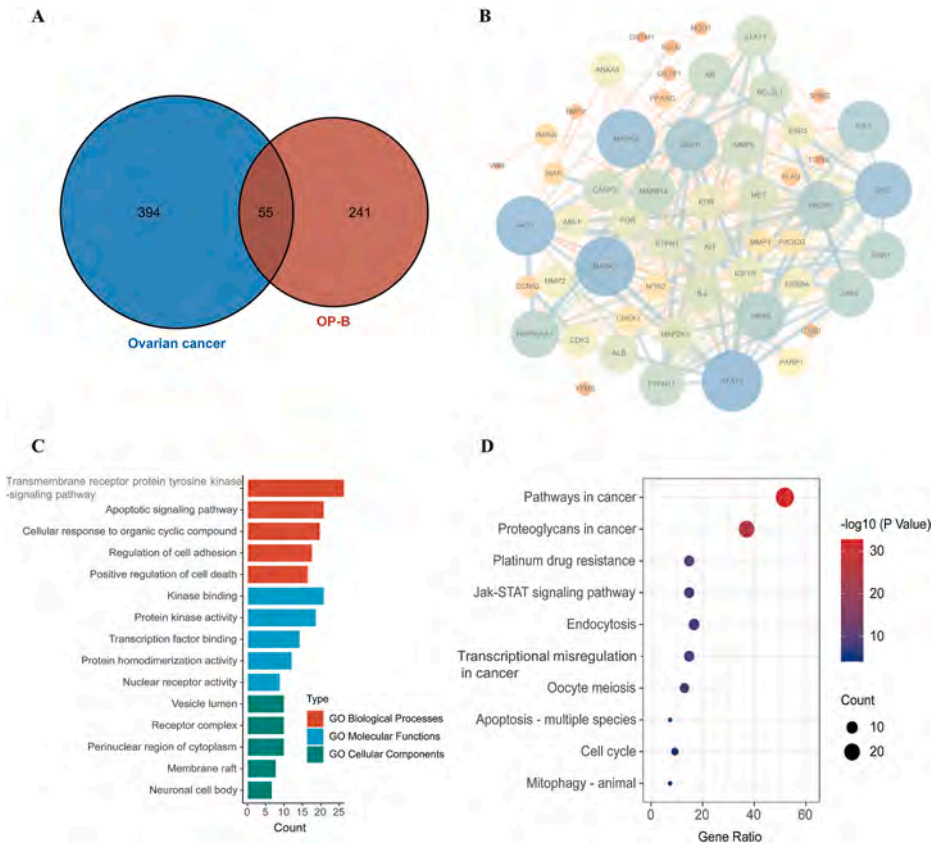

Fig. 2. (A)Venn diagram indicating further intersection of OP-B target genes (red circle) and OC related genes (blue circle). (B)Protein-protein interaction (PPI) network. The nodes get larger with increasing degree. The Edges get thicker with closer association between proteins. (C)Gene ontology enrichment analysis of identified related targets. Red rectangle biological process, blue rectangle cellular component, green rectangle molecular function. (D)KEGG Pathway analysis for identified related targets. (For interpretation of the references to colour in this figure legend, the reader is referred to the Web version of this article.)

Therefore, these data indicated that OP-B exerted its suppressed effects against OC and was closely linked with the activity of these signaling pathways.

3.4. Effects of OP-B on SKOV3 and A2780 ovarian cancer cell viability

Cell viability assays were performed to evaluate the cytotoxic effects of OP-B on SKOV3 and A2780 cells. Compared with the control group, ovarian cancer cells following OP-B treatment demonstrated a significant decrease in cell viability in a concentration and time dependent manner (Fig. 3A, SKOV3:24H IC50: 27.61 μM, 48H IC50: 22.58 μM) (Fig. 3B, A2780:24H IC50: 20.28 μM, 48H IC50: 19.45 μM). At the concentration of 10, 20 μM, Cisplatin had a similar inhibition effect as OP-B at the same condition ($P > 0.05$). Furthermore, at the concentration of 30, 40 μM, exposure to OP-B evoked stronger suppressive effects than cisplatin ($P < 0.05$). These data suggested that OP-B could inhibit OC cells viability and proliferation.

3.5. Effects of OP-B on SKOV3 and A2780 ovarian cancer cell migration

Under the microscope, it was found that the number of SKOV3 cells decreased significantly, and the average number of cells per visual field in the control group was 143.39 ± 5.89 cells, while that in the 15 and 20 μM OP-B groups were 132.00 ± 7.27, 97.67 ± 6.98 cells (Fig. 3D). Similarly, the average number of A2780 cells in the control group was 183.67 ± 4.92 cells, while that in the OP-B groups were 95.17 ± 5.78 and 73.00 ± 7.78 cells (Fig. 3D). The results of the transwell chamber test showed that the migration capacity of all experimental groups was significantly lower than that of the control group, the migration of cells decreased with increasing drug concentration, and the difference was statistically significant ($P < 0.001$).

3.6. Effects of OP-B on SKOV3 and A2780 ovarian cancer cellular apoptosis

In order to determine whether OP-B-induced cytotoxicity was due to activated apoptosis, the apoptotic rates were examined by flow cytometry after staining with Annexin V-FITC and PI. The Annexin V (+)/PI (−) population which are presented in the lower right quadrant indicates early apoptosis. Annexin V (+)/PI (+) population presented in the upper right quadrant indicates late apoptosis, respectively. The total apoptosis rate, including early and late apoptosis populations, was calculated.

Flow cytometry analysis showed that the group of OP-B increased both early and late-stage apoptosis (Fig. 4A). As shown in Fig. 4B, the total apoptotic SKOV3 cells increased from 7.18 ± 0.15% in control group to 70.87 ± 0.47% in cells treated with 30 μM OP-B for 24h ($P < 0.01$). The total apoptosis rates of SKOV3 cells induced by 0, 10, 20, and 30 μM of OP-B treatment for 48h were 15.71 ± 1.42, 21.22 ± 0.47, 37.75 ± 1.02, and 84.90 ± 0.50%, respectively. Our data showed that OP-B treatment significantly increased the percentage of apoptosis SKOV3 cells in a dose-dependent manner. As shown in Fig. 4B, 20 and 30 μM OP-B induced apoptosis in A2780 cells in a time and dose dependent manner, inducing a maximum of 39.76 ± 1.55%–86.56 ± 0.06 of apoptosis.

3.7. Effects of OP-B on SKOV3 and A2780 ovarian cancer cell cycle

To determine whether proliferation inhibition of OP-B on SKOV3 and A2780 cells was attributed to the cell cycle arrest, the cell cycle distribution was analyzed by flow cytometry after PI stain (Fig. 5). After treatment with 20 or 30 μM of OP-B, the number of SKOV3 cells in the G0/G1 phase decreased to 24.93 ± 1.33 or 14.10 ± 2.55% ($P < 0.05$), respectively, which in the control group was 46.00 ± 7.75%. Meanwhile, the cells in the G2/M phase increased from 26.57 ± 4.94 (control

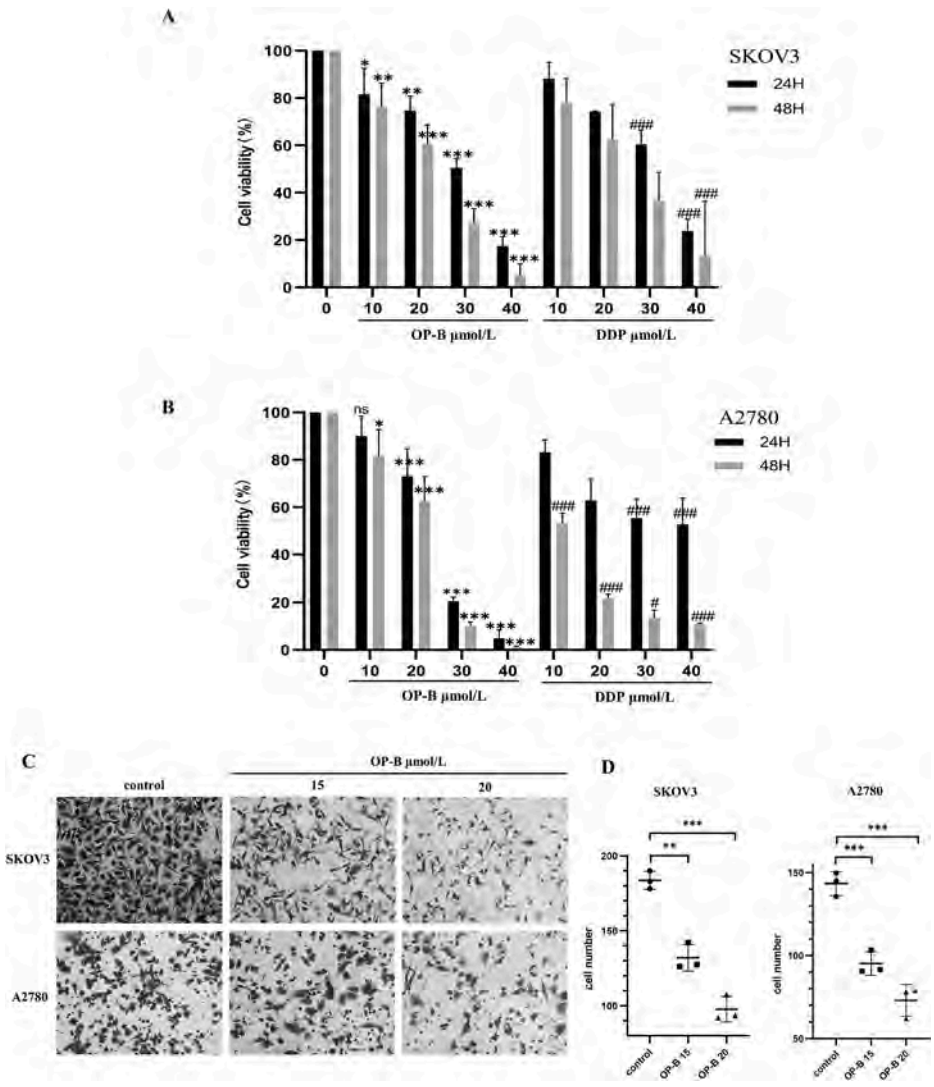

Fig. 3. OP-B inhibits cell viability and migration of SKOV3 and A2780 cells. Viability of SKOV3 (A) and A2780 (B) cells following 24h and 48h incubation with the indicated doses of OP-B and DDP. All data are presented as mean ± standard deviation (SD; n=3). ns $P > 0.05$, *$P < 0.05$, **$P < 0.01$, ***$P < 0.001$ versus 0 μM group; #$P < 0.05$, ###$P < 0.001$ versus the DDP group. (C) Transwell migration assay was performed to determine the effect of OP-B on cell migration. Migrating cells were photographed (× 200 magnification). (D) Quantification of the migrated ovarian cancer cells. All data are presented as mean ± SD (n=3), *$P < 0.05$, **$P < 0.01$, ***$P < 0.001$ versus the control group.

group) to 47.10 ± 2.24 or 52.87 ± 5.70% under 20 or 30 μM of OP-B treatment, respectively ($P < 0.05$). The results suggested that OP-B induced cell cycle arrest at G2/M phase in SKOV3 cells. On the contrary, the number of A2780 cells in the G0/G1 phase increased from 49.16 ± 0.36 (control group) to 52.30 ± 0.63 or 53.00 ± 1.64% under 10 or 20 μM of OP-B treatment, respectively ($P < 0.05$). The results suggested that OP-B induced cell cycle arrest at G0/G1 phase in A2780 cells.

3.8. Effects of OP-B on potential targets in vitro

To verify the results based on the network pharmacology analysis, we chose the high related target STAT3 for experimental validation. The results of qRT-PCR showed that the treatment with OP-B slightly reduced the gene expression of STAT3 in SKOV3 and A2780 cells ($P > 0.05$, Fig. 6B). The results of Western blot indicated that OP-B significantly decreased the phosphorylation levels of STAT3 ($P < 0.05$), whilst total STAT3 protein levels were not changed ($P > 0.05$) (Fig. 6C and D). Taken together, these results suggested that the effect of OP-B in OC might be related to the STAT3 signal transduction pathways in human OC cells.

3.9. Effect of OP-B on ovarian cancer in nude mice in vivo

To investigate the in vivo antitumor effects of OP-B, ovarian cancer xenografts in nude mice were established using SKOV3 cells. The results showed that the tumor volume of mice treated with OP-B 75 mg/kg on day 18, 21 were markedly lower than the control group ($P < 0.05$, Fig. 7A). The tumor inhibition ratio of OP-B 15 mg/kg and 75 mg/kg group were 25.45% and 45.69%, respectively. Moreover, body weights of all nude mice were not significantly different for the duration of the experiment ($P > 0.05$, Fig. 7B). The xenograft tumors in each group of nude mice were shown in Fig. 7D. Pathological examination was used to evaluate toxicity of OP-B by HE staining. Microscopically, no significant pathological changes in heart, liver, lung, and kidney were observed in 15 mg/kg OP-B group (Fig. 7E). In 75 mg/kg OP-B group, apart from mild congestion in liver and lung of one nude mouse, none of other samples showed evidence of cell degeneration, necrosis, or infiltration of inflammatory factors in heart, liver, lung, and kidney. These results showed that OP-B could inhibit tumor growth in vivo.

4. Discussion

Some natural products derived from plants have demonstrated anticancer properties with fewer side effects compared to current chemical synthetic drugs. Complex diseases, such as cancer, are characterized by dysregulation of multiple cellular functions that interact in a complex network environment (Wang et al., 2014); no protein can account for all disease states. Network pharmacology is a powerful tool that can explain the function of a complicated biological system, which brings theoretical and methodological significance to drug design (Hopkins, 2008). As a

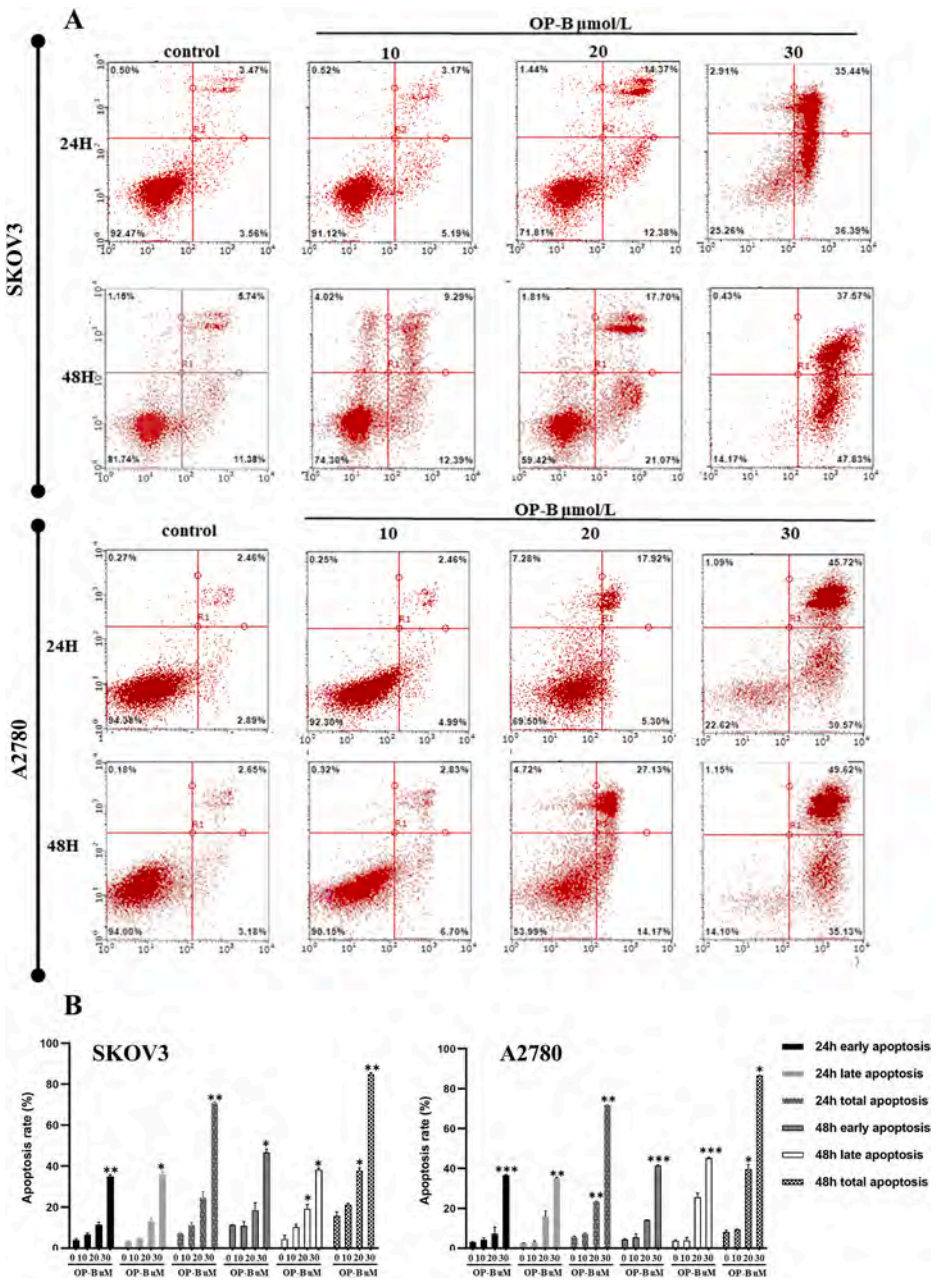

Fig. 4. OP-B induces apoptosis in SKOV3 and A2780 cells. (A)Flow cytometric analysis of Annexin V/PI double staining in SKOV3 and A2780 cells treated with various concentrations of OP-B for 24h and 48h. Lower left quadrant: live cells; lower right quadrant: early apoptosis; upper right quadrant: late apoptosis; upper left quadrant: necrotic cells. (B) Quantification of the early apoptosis, late apoptosis, and total apoptosis rates (early apoptosis rates + late apoptosis rates). All data are presented as mean ± SD (n=3), *P < 0.05, **P < 0.01, ***P < 0.001 versus the control group.

Chinese herbal, the application of Maidong on "nourishing Yin and promoting fluid production" has a long history (M.-H. Chen et al., 2016b). Clinically, Maidong is used medication on cardiovascular disease, inflammation, assistant cancer chemotherapy and food supplements (Zhang, Lu et al., 2019). OP-B, isolated from Maidong, has been shown to possess antitumor properties through various mechanisms(He et al., 2018). In the present study, we undertook network pharmacology analysis coupled with experimental validation to investigate the effects and mechanism of OP-B against OC, aimed to develop novel effective anti-cancer drugs.

An "OP-B-targets-OC" PPI network was constructed to identify the potential targets and mechanisms of OP-B in the treatment of OC. This systematic approach revealed that 10 key potential targets related to OP-B, such as STAT3, c-Jun, c-Myc, CCND1, MMP9 and JAK2, were closely linked with OC. The results of enrichment analysis showed that OP-B may participate in the positive regulation of cell death by regulating JAK-STAT signaling pathway, apoptotic signaling pathway, cell cycle, cell adhesion regulation, etc. Clinically, increasing evidence indicates that the activation of the STAT3 pathway has significant correlation with development of OC, suggesting the importance of STAT3 as potential therapeutic targets for cancer therapy (Lu et al., 2019) (Wu et al., 2019). In this study, we evaluated STAT3 expression in SKOV3 and A2780 cells. The results showed that OP-B could decrease STAT3 phosphorylation levels. Therefore, our results revealed that OP-B plays a significant anti-OC role, which is mediated by the STAT3 pathway. We observed that OP-B exhibited a significant cytotoxic effect both on SKOV3 and A2780 cells. The cellular morphology changes and the cells shrunk into spheres and floated after the OP-B treatment. The suppressive effects of 30, 40 μM OP-B is stronger than that of cisplatin, which is currently the most effective first-line drug for OC. This suggested that OP-B acted as an alternative chemotherapy for OC.

Apoptosis is a spontaneous, gene-controlled, and orderly cell death, which can be initiated by a variety of extracellular stimuli, such as nutrient supply, DNA damage, and environmental stress (Pistritto et al., 2016). It is a stage-dependent process such as early and late apoptotic events, as well as apoptotic cells undergo changes in morphology and

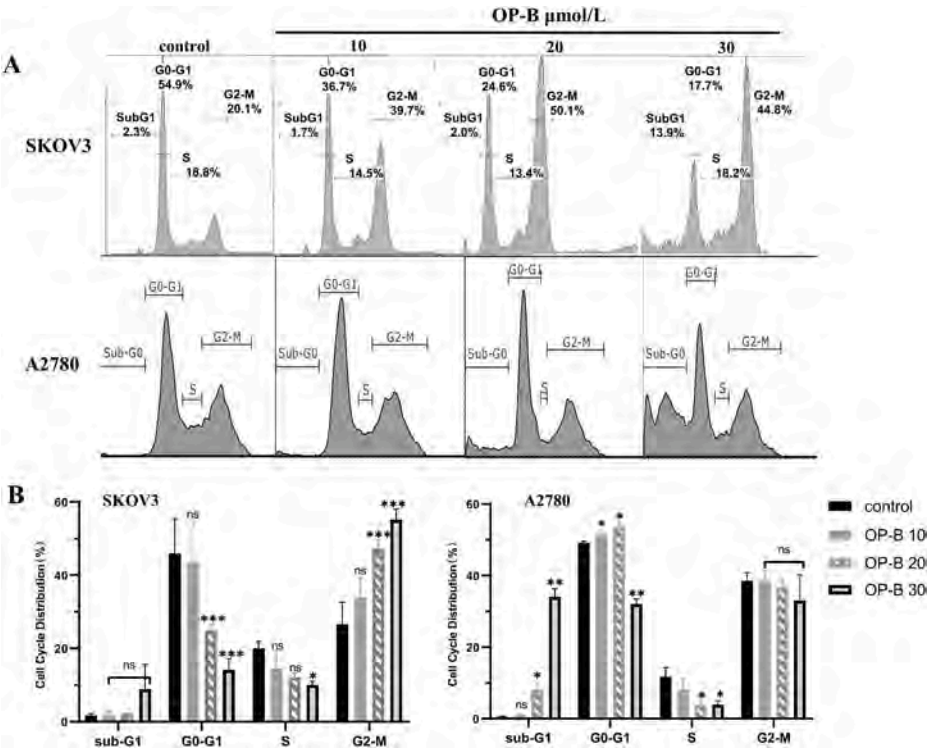

Fig. 5. OP-B induces cell cycle arrest in SKOV3 and A2780 cells. Cell cycle analysis revealed that OP-B arrested cells at the G2/M checkpoint in SKOV3 cells and at the G0/G1 checkpoint in A2780 cells. Cells were incubated with the indicated dose of OP-B for 24 h, stained with Propidium iodide (PI), and DNA content was analyzed via flow cytometry. All data are presented as mean ± SD (n=3), *P < 0.05, **P < 0.01, ***P < 0.001 versus the control group.

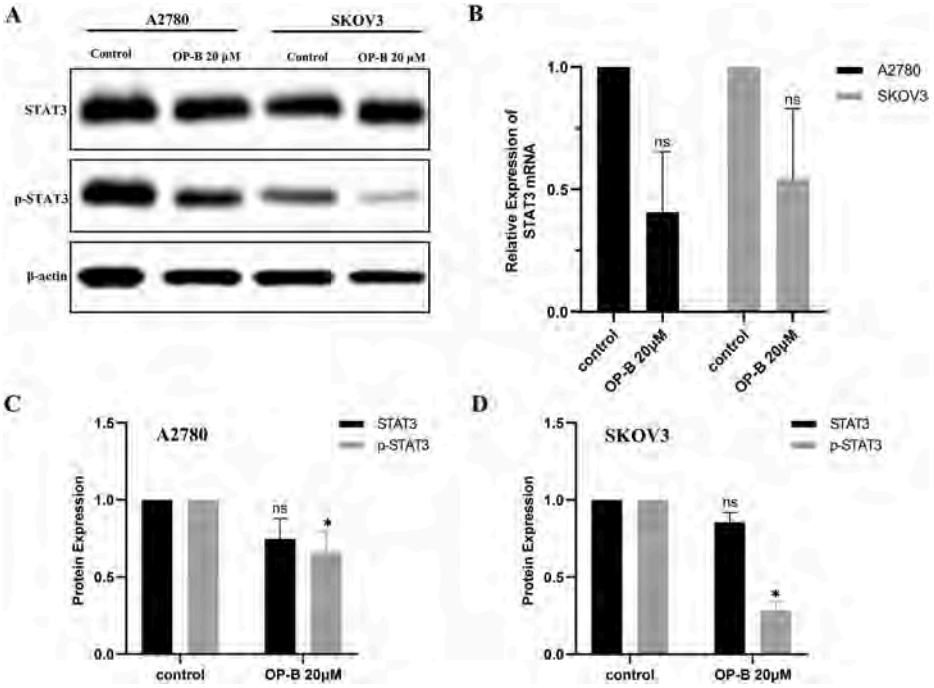

Fig. 6. OP-B down-regulates STAT3 expression in human OC cells. (A, C, D) Western blot analysis of STAT3, and p-STAT3 in SKOV3 and A2780 cells. (B) STAT3 mRNA expression evaluation by qRT-PCR in SKOV3 and A2780 cells. Data are presented as mean ± SD (n=3), *P < 0.05, **P < 0.01, ***P < 0.001 versus the control group.

biochemical events. According to the results, SKOV3 and A2780 cells treated with 20, 30 μM OP-B resulted in high proportion of apoptotic cells. We found that OP-B mainly increased the late apoptosis in low dosage, and induced early and late apoptosis in high dosage. Gao Guang-Yi et al. have found that OP-B can increase the total apoptosis rate of colon cancer cells HT29 and HCT-116 after 48 h treatment (Gao et al., 2018). In previous studies, only the total apoptosis of cancer cells was discussed, and the different changes in the proportion of early and

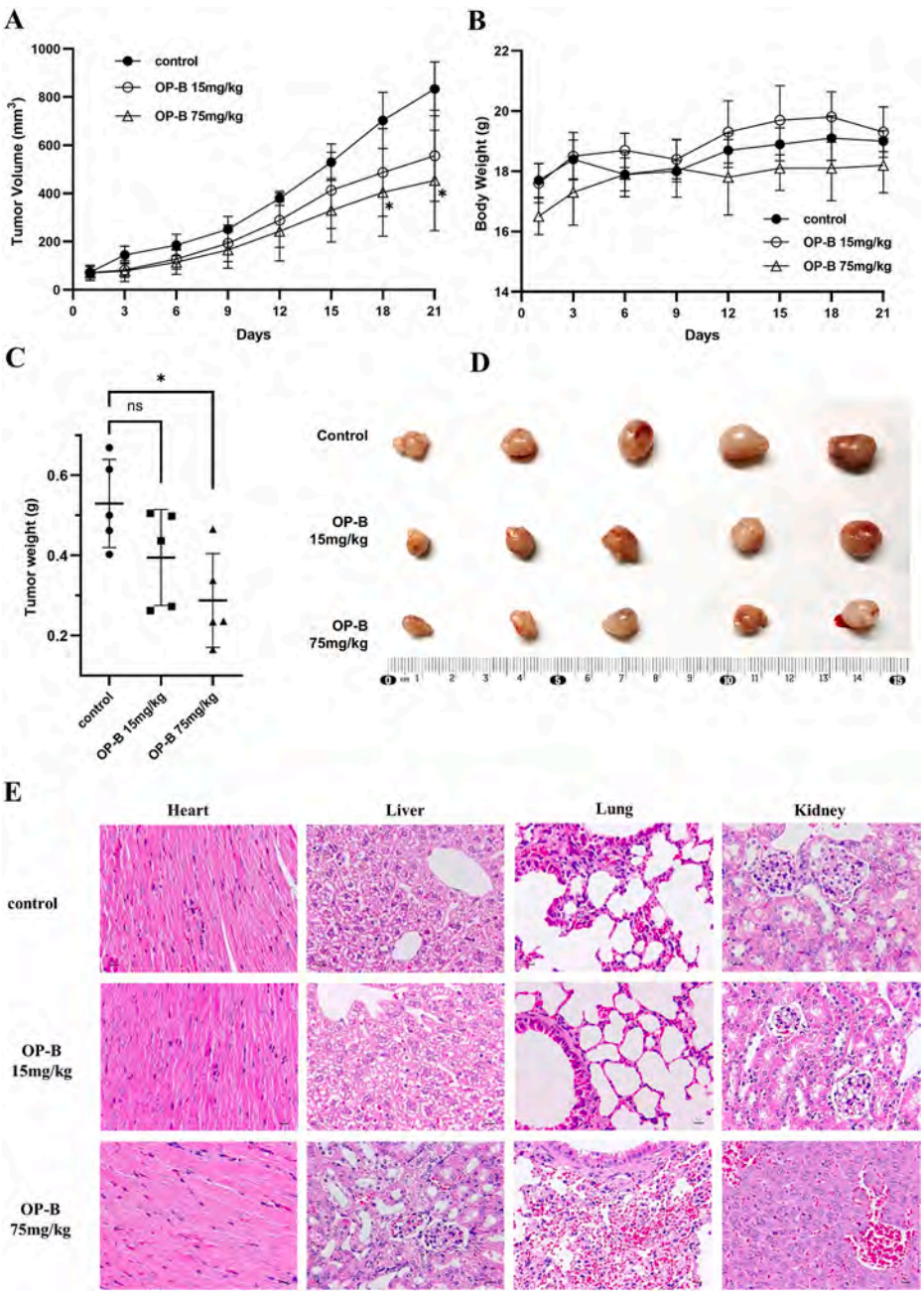

Fig. 7. OP-B suppresses the growth of tumors in nude mice subcutaneously implanted with SKOV3 cells. (A, C) Growth curve and Tumor weights of xenograft tumor in nude mice. (B) The weight of nude mice from each group did not change significantly during the experiment. (D) Representative image of xenograft tumor formation in nude mice. Data are presented as mean ± SD (n=5), *P < 0.05 versus the control group. (E) HE staining analysis was performed to examine the pathological changes of the heart, liver, lungs, and kidneys of the mice from different treatment groups.

late apoptosis were not analyzed.

Cell cycle arrest is a critical aspect of the anti-proliferative activity (Evan and Vousden, 2001). Growth arrest occurs usually in the G1 or G2/M phases of the cell cycle. The transition between one cycle phase and another occurs in order and is regulated by a variety of cell cycle regulators, the most prominent of which are cyclins and their associated CDKs(Kastan and Bartek, 2004). In this study, OP-B induced cell cycle arrest at G2/M phases in SKOV3 cells and that at G0/G1 phase in A2780 cells. The position and duration of cell cycle arrests in SKOV3 and A2780 cells were different. Similarly, in non-small cell lung cancer, OP-B was also observed to induce G2/M cycle arrest in A549 cells (M. Chen et al., 2016a), while blocking NCI-H157 and NCI-H460 cells in G0/G1 phase (Chen et al., 2013). Different tumor stage and histological subtypes have different clinical characteristics. SKOV3 cells represent adenocarcinoma, and A2780 cells represent undifferentiated cancer (Beaufort et al., 2014). Its underlying mechanism is cell type-dependent.

Advanced OC is always characterized by extensive local aggression, cervical lymph node metastasis and distant metastasis (Narod, 2016). The results showed that compared with the control group, 15, 20 μM OP-B could significantly inhibit the migrated number of SKOV3 and A2780 cells in a dose-dependent manner. As in this study, researchers have found that OP-B can inhibit the migration and invasion of gastric cancer MGC-803 cells (Yang et al., 2019) and non-small cell lung cancer A549 cells (Chen et al., 2018) by down-regulating the MMPs protein and epithelial-mesenchymal transition (EMT) pathway.

Experimental tumor models are essential preclinical step for the development and evaluation of cancer chemotherapy strategies (Magnotti and Marasco, 2018). Previous studies have shown that 15, 75 mg/kg OP-B can significantly inhibit the growth of colon cancer cell in nude mice (Gao et al., 2018). While 37.5, 75 mg/kg OP-B can inhibit the growth and lung metastasis of A549 xenografts nude mice (M. Chen et al., 2016a) (Chen et al., 2018). We used 15 and 75 mg/kg of OP-B in SKOV3 xenografts nude mice to detect its effect in vivo. Consistent with the results in vitro, subcutaneous xenograft study showed that growth of

xenografted tumor was dramatically suppressed after treating with 75 mg/kg OP-B for three weeks. Apart from mild congestion in liver and lung of one nude mouse, none of other samples showed evidence of cell degeneration, necrosis, or infiltration of inflammatory factors in heart, liver, lung, and kidney. In other words, there were no significant histopathological changes in tissue sections from the mice heart, liver, lung, and kidney. Due to the time and technical limitation, pre-toxicological experiment or pharmacokinetic experiment could not be done. Therefore, the therapeutic dose of OP-B should be further investigated until an optimal dose is identified, for use in OC, in order to achieve an optimal therapeutic efficacy and avoid potential toxicity.

In summary, our results showed that OP-B was able to suppress ovarian cancer in vitro and in vivo by inhibiting STAT3 pathway, which might widen the anti-cancer spectrum of OP-B. With the network pharmacology, it was concluded that OP-B may play an anti-OC effect through multiple pathway mechanisms such as regulating apoptotic signaling pathways to promote cell apoptosis, regulating cell adhesion to inhibit cell metastasis, and blocking cell cycles to disrupt mitosis.

In further studies, it would be interesting to explore whether the combination of OP-B and cisplatin can enhance antitumor efficiency and reduce toxic side effects of cisplatin. In addition, the pharmacokinetics of OP-B remains to be ascertained. The main limitation of OP-B for its translation into clinics is its low solubility. Liposomes, micelles, polymer nanoparticles, or microparticles may optimize the bioavailability and the bio-distribution of the drug (George et al., 2019). This needs to be further explored.

5. Conclusion

The pharmacological mechanism by which OP-B inhibited OC was investigated with the combination of network pharmacology prediction and experimental validation. This study demonstrated, for the first time, that OP-B could efficiently suppress OC cellular proliferation, migration and induce apoptosis, cell cycle arrest mainly via the regulation of STAT3 signaling pathway. In addition, OP-B could inhibit liver tumor growth of subcutaneously implanted OC in nude mice, without exhibiting noticeable side effects. To sum up, the data available from this study provided initial evidence that OP-B may be a promising anti-cancer medicine, which can be developed as a therapeutic option for the treatment of ovarian cancer.

Funding

This research is financially supported by Sichuan Science and Technology program (grant number 2021YFS0126) of Sichuan Province in China.

CRediT authorship contribution statement

Shuang Yuan: Methodology, Software, Data curation, Writing – original draft. **Yuanyuan Xu:** Methodology. **Tao Yi:** Supervision, Formal analysis. **Hongjing Wang:** Supervision, Writing – review & editing.

Declaration of competing interest

The authors declare that they have no known competing financial interests or personal relationships that could have appeared to influence the work reported in this paper.

References

Armstrong, D.K., Alvarez, R.D., Bakkum-Gamez, J.N., Barroilhet, L., Behbakht, K., Berchuck, A., Chen, L.-M., Cristea, M., DeRosa, M., Eisenhauer, E.L., Gershenson, D. M., Gray, H.J., Grisham, R., Hakam, A., Jain, A., Karam, A., Konecny, G.E., Leath, C. A., Liu, J., Mahdi, H., Martin, L., Matei, D., McHale, M., McLean, K., Miller, D.S., O'Malley, D.M., Percac-Lima, S., Ratner, E., Remmenga, S.W., Vargas, R., Werner, T. L., Zsiros, E., Burns, J.L., Engh, A.M., 2021. Ovarian cancer, version 2.2020, NCCN clinical practice guidelines in oncology. J. Natl. Compr. Cancer Netw. JNCCN 19, 191–226. https://doi.org/10.6004/jnccn.2021.0007.

Beaufort, C.M., Helmijr, J.C.A., Piskorz, A.M., Hoogstraat, M., Ruigrok-Ritstier, K., Besselink, N., Murtaza, M., van IJcken, W.F.J., Heine, A.A.J., Smid, M., Koudijs, M.J., Brenton, J.D., Berns, E.M.J.J., Helleman, J., 2014. Ovarian cancer cell line panel (OCCP): clinical importance of in vitro morphological subtypes. PLoS One 9, e103988. https://doi.org/10.1371/journal.pone.0103988.

Chen, M., Du, Y., Qui, M., Wang, M., Chen, K., Huang, Z., Jiang, M., Xiong, F., Chen, J., Zhou, J., Jiang, F., Yin, L., Tang, Y., Ye, L., Zhan, Z., Duan, J.-A., Fu, H.-A., Zhang, X., 2013. Ophiopogonin B-induced autophagy in non-small cell lung cancer cells via inhibition of the PI3K/Akt signaling pathway. Oncol. Rep. 29, 430–436. https://doi.org/10.3892/or.2012.2131.

Chen, M., Guo, Y., Zhao, R., Wang, X., Jiang, M., Fu, H., Zhang, X., 2016a. Ophiopogonin B induces apoptosis, mitotic catastrophe and autophagy in A549 cells. Int. J. Oncol. 49, 316–324. https://doi.org/10.3892/ijo.2016.3514.

Chen, M.-H., Chen, X.-J., Wang, M., Lin, L.-G., Wang, Y.-T., 2016b. Ophiopogon japonicus-A phytochemical, ethnomedicinal and pharmacological review. J. Ethnopharmacol. 181, 193–213. https://doi.org/10.1016/j.jep.2016.01.037.

Chen, X., Yan, C.C., Zhang, Xiaotian, Zhang, Xu, Dai, F., Yin, J., Zhang, Y., 2016c. Drug-target interaction prediction: databases, web servers and computational models. Briefings Bioinf. 17, 696–712. https://doi.org/10.1093/bib/bbv066.

Chen, M., Hu, C., Guo, Y., Jiang, R., Jiang, H., Zhou, Y., Fu, H., Wu, M., Zhang, X., 2018. Ophiopogonin B suppresses the metastasis and angiogenesis of A549 cells in vitro and in vivo by inhibiting the EphA2/Akt signaling pathway. Oncol. Rep. 40, 1339–1347. https://doi.org/10.3892/or.2018.6531.

Demain, A.L., Vaishnav, P., 2011. Natural products for cancer chemotherapy. Microb. Biotechnol. 4, 687–699. https://doi.org/10.1111/j.1751-7915.2010.00221.x.

Deorukhkar, A., Krishnan, S., Sethi, G., Aggarwal, B.B., 2007. Back to basics: how natural products can provide the basis for new therapeutics. Expet Opin. Invest. Drugs 16, 1753–1773. https://doi.org/10.1517/13543784.16.11.1753.

Evan, G.I., Vousden, K.H., 2001. Proliferation, cell cycle and apoptosis in cancer. Nature 411, 342–348. https://doi.org/10.1038/35077213.

Gao, G.-Y., Ma, J., Lu, P., Jiang, X., Chang, C., 2018. Ophiopogonin B induces the autophagy and apoptosis of colon cancer cells by activating JNK/c-Jun signaling pathway. Biomed. Pharmacother. 108, 1208–1215. https://doi.org/10.1016/j.biopha.2018.06.172.

George, A., Shah, P.A., Shrivastav, P.S., 2019. Natural biodegradable polymers based nano-formulations for drug delivery: a review. Int. J. Pharm. 561, 244–264. https://doi.org/10.1016/j.ijpharm.2019.03.011.

He, B., Zhou, X., Shi, D., Cheng, G., 2018. Progress on anti-tumor effects and mechanisms of ophiopogonin B. Chin. Arch. Tradit. Chin. Med. 36, 2911–2914.

Hopkins, A.L., 2008. Network pharmacology: the next paradigm in drug discovery. Nat. Chem. Biol. 4, 682–690. https://doi.org/10.1038/nchembio.118.

Kastan, M.B., Bartek, J., 2004. Cell-cycle Checkpoints Canc. 432, 8.

Kibble, M., Saarinen, N., Tang, J., Wennerberg, K., Mäkelä, S., Aittokallio, T., 2015. Network pharmacology applications to map the unexplored target space and therapeutic potential of natural products. Nat. Prod. Rep. 32, 1249–1266. https://doi.org/10.1039/c5np00005j.

Kuroki, L., Guntupalli, S.R., 2020. Treatment of epithelial ovarian cancer. BMJ 371, m3773. https://doi.org/10.1136/bmj.m3773.

Lee, J.-M., Minasian, L., Kohn, E.C., 2019. New strategies in ovarian cancer treatment. Cancer 125 (Suppl. 24), 4623–4629. https://doi.org/10.1002/cncr.32544.

Lheureux, S., Braunstein, M., Oza, A.M., 2019. Epithelial ovarian cancer: evolution of management in the era of precision medicine. CA. Canc. J. Clin. 69, 280–304. https://doi.org/10.3322/caac.21559.

Lu, L.-Y., Zheng, G.-Q., Wang, Y., 2014. An overview of systematic reviews of shenmai injection for healthcare. Evid.-Based Compl. Altern. Med. ECAM 2014, 840650. https://doi.org/10.1155/2014/840650.

Lu, T., Bankhead, A., Ljungman, M., Neamati, N., 2019. Multi-omics profiling reveals key signaling pathways in ovarian cancer controlled by STAT3. Theranostics 9, 5478–5496. https://doi.org/10.7150/thno.33444.

Lyu, C., Kang, C., Kang, L., Yang, J., Wang, S., He, Y., Deng, A., Wang, H., Huang, L., Guo, L., 2020. Structural characterization and discrimination of Ophiopogon japonicas (Liliaceae) from different geographical origins based on metabolite profiling analysis. J. Pharmaceut. Biomed. Anal. 185, 113212 https://doi.org/10.1016/j.jpba.2020.113212.

Magnotti, E., Marasco, W.A., 2018. The latest animal models of ovarian cancer for novel drug discovery. Expet Opin. Drug Discov. 13, 249–257. https://doi.org/10.1080/17460441.2018.1426567.

Narod, S., 2016. Can advanced-stage ovarian cancer be cured? Nat. Rev. Clin. Oncol. 13, 255–261. https://doi.org/10.1038/nrclinonc.2015.224.

Pistritto, G., Trisciuoglio, D., Ceci, C., Garufi, A., D'Orazi, G., 2016. Apoptosis as anticancer mechanism: function and dysfunction of its modulators and targeted therapeutic strategies. Aging 8, 603–619. https://doi.org/10.18632/aging.100934.

Siegel, R.L., Miller, K.D., Jemal, A., 2020. Cancer statistics, 2020. CA. Canc. J. Clin. 70, 7–30. https://doi.org/10.3322/caac.21590.

Sung, H., Ferlay, J., Siegel, R.L., Laversanne, M., Soerjomataram, I., Jemal, A., Bray, F., 2021. Global cancer statistics 2020: GLOBOCAN estimates of incidence and mortality worldwide for 36 cancers in 185 countries. CA. Canc. J. Clin. 71, 209–249. https://doi.org/10.3322/caac.21660.

Wang, C.-Y., Bai, X.-Y., Wang, C.-H., 2014. Traditional Chinese medicine: a treasured natural resource of anticancer drug research and development. Am. J. Chin. Med. 42, 543–559. https://doi.org/10.1142/S0192415X14500359.

Wu, C.-J., Sundararajan, V., Sheu, B.-C., Huang, R.Y.-J., Wei, L.-H., 2019. Activation of STAT3 and STAT5 signaling in epithelial ovarian cancer progression: mechanism and

therapeutic opportunity. Cancers 12, E24. https://doi.org/10.3390/cancers12010024.

Xu, Q.-J., Hou, L.-L., Hu, G.-Q., Xie, S.-Q., 2013. Molecular mechanism of ophiopogonin B induced cellular autophagy of human cervical cancer HeLa cells. Yao Xue Xue Bao 48, 855–859.

Yan, Y.-B., Tian, Q., Zhang, J.-F., Xiang, Y., 2020. Antitumor effects and molecular mechanisms of action of natural products in ovarian cancer. Oncol. Lett. 20, 141. https://doi.org/10.3892/ol.2020.12001.

Yang, J., Sun, C., Jiang, Z., Zhao, F., Zeng, X., Feng, Q., Wu, M., 2019. Effects of ophiopogonin B on invasion and migration of human gastric cancer MGC-803 cells. China J. Tradit. Chin. Med. Pharm. 34, 2742–2745.

Zhang, W., Zhang, Q., Jiang, Y., Li, F., Xin, H., 2016. Effects of ophiopogonin B on the proliferation and apoptosis of SGC-7901 human gastric cancer cells. Mol. Med. Rep. 13, 4981–4986. https://doi.org/10.3892/mmr.2016.5198.

Zhang, L., Luo, Z., Cui, S., Xie, L., Yu, J., Tang, D., Ma, X., Mou, Y., 2019. Residue of paclobutrazol and its regulatory effects on the secondary metabolites of ophiopogon japonicas. Molecules 24 (19), 3504. https://doi.org/10.3390/molecules24193504.

Zhao, M., Xu, W.-F., Shen, H.-Y., Shen, P.-Q., Zhang, J., Wang, D.-D., Xu, H., Wang, H., Yan, T.-T., Wang, L., Hao, H.-P., Wang, G.-J., Cao, L.-J., 2017. Comparison of bioactive components and pharmacological activities of ophiopogon japonicas extracts from different geographical origins. J. Pharmaceut. Biomed. Anal. 138, 134–141. https://doi.org/10.1016/j.jpba.2017.02.013.